

Appl. Phys. B – special issue ‘Nano optics’ – manuscript No.
 (will be inserted by the editor)

Electromagnetic field correlations near a surface with a nonlocal optical response

Carsten Henkel^{1*}, Karl Joulain²

¹Institut für Physik, Universität Potsdam, Germany,

²Laboratoire d’Etudes Thermiques, Ecole Nationale Supérieure de Mécanique Aéronautique, Poitiers, France

23 March 2006

Abstract The coherence length of the thermal electromagnetic field near a planar surface has a minimum value related to the nonlocal dielectric response of the material. We perform two model calculations of the electric energy density and the field’s degree of spatial coherence. Above a polar crystal, the lattice constant gives the minimum coherence length. It also gives the upper limit to the near field energy density, cutting off its $1/z^3$ divergence. Near an electron plasma described by the semiclassical Lindhard dielectric function, the corresponding length scale is fixed by plasma screening to the Thomas-Fermi length. The electron mean free path, however, sets a larger scale where significant deviations from the local description are visible.

PACS: 42.25.Kb Coherence – 07.79.Fc Near-field scanning optical microscopes – 44.40.+a Thermal radiation – 78.20.-e Optical properties of bulk materials and thin films

1 Introduction

Thermal electromagnetic radiation in vacuum, as described by the celebrated blackbody spectrum discovered by Max Planck [1], is usually taken as a typical example of incoherent radiation. This is not quite true, however: if the radiation is detected at a given frequency, it is spatially coherent on a scale set by the wavelength [2, 3]. When one approaches a macroscopic object, the radiation spectrum and its coherence is profoundly changed, depending on the properties of the object. For example, if the object supports resonant modes like surface plasmon polaritons, the field is coherent across the propagation length of these modes [4]. The opposite case is possible as well: the coherence length becomes comparable to the observation distance, much smaller than the wavelength, close to an absorbing object with a local

* email: Carsten.Henkel@physik.uni-potsdam.de

dielectric function [5]. It has been suggested already by Rytov and colleagues that this behaviour is an artefact because at some small scale, nonlocal effects must come into play [2]. This is what we discuss in this paper in a semi-quantitative way. We use two models for nonlocal dielectric functions and identify the scale for the field's coherence length using explicit asymptotic formulas. A nonlocal dielectric response is of primary importance for semiconductor quantum wells, see for example Ref.[6], but the issue of spatial coherence has not been analyzed in this context, to our knowledge.

We focus on the spatial coherence of the electromagnetic field at nanometer distance in the vacuum (medium 1) above a solid material (medium 2). We chose a planar geometry which is sufficiently simple to allow for an essentially analytical description, thus avoiding the need for extensive numerics. On the other hand, many effects have been discussed in this setting: the fluorescence rate of molecules near metals and thin films [7], scanning near-field microscopy of sub-wavelength objects deposited on a substrate [8], the momentum exchange between a tip and a sample (related to the Casimir force, see, e.g., [9]) and the energy exchange between a tip and a sample [10, 11, 12, 13].

2 Basic notation

2.1 Field correlations

The spatial coherence of the electric field is determined by the two-point expectation value [14]

$$\langle E_i(\mathbf{r}_1, t_1) E_j(\mathbf{r}_2, t_2) \rangle = \int \frac{d\omega}{2\pi} \mathcal{E}_{ij}(\mathbf{r}_1, \mathbf{r}_2; \omega) e^{i\omega(t_1 - t_2)}, \quad (1)$$

where the average is taken in a stationary statistical ensemble (thermal equilibrium in the simplest case). We focus in the following on the cross-correlation spectrum $\mathcal{E}_{ij}(\mathbf{r}_1, \mathbf{r}_2; \omega)$ and a frequency in the infrared to visible range. Far from any sources and in global equilibrium, the corresponding wavelength $\lambda = 2\pi c/\omega$ sets the scale for the field's spatial coherence length: the cross-correlations tend to zero if the distance $|\mathbf{r}_1 - \mathbf{r}_2|$ exceeds λ . In the vicinity of a source, the coherence length ℓ_{coh} significantly differs from λ , as Henkel and co-workers have shown previously [5], and it changes with the observation point.

The spectrally resolved electric energy density is given by the trace

$$u_E(\mathbf{r}; \omega) = \frac{\varepsilon_0}{2} \sum_i \mathcal{E}_{ii}(\mathbf{r}, \mathbf{r}; \omega), \quad (2)$$

and its value in thermal equilibrium allows to define an electric, local density of states, as discussed in more detail by Joulain and co-workers [15]. The normalized tensor

$$c_{ij}(\mathbf{r}_1, \mathbf{r}_2; \omega) = \frac{\frac{1}{2} \varepsilon_0 \mathcal{E}_{ij}(\mathbf{r}_1, \mathbf{r}_2; \omega)}{\sqrt{u_E(\mathbf{r}_1; \omega) u_E(\mathbf{r}_2; \omega)}}, \quad (3)$$

to be considered below, allows to introduce a spatial degree of coherence. In the following, we call a “coherence function” both, $\mathcal{E}_{ij}(\mathbf{r}_1, \mathbf{r}_2; \omega)$ and Eq.(3). Definitions for a degree of polarization based on this 3×3 matrix (with $\mathbf{r}_1 = \mathbf{r}_2$) have been put forward as well, see [16, 17]. For the sake of simplicity, we suppress the frequency arguments in the following.

2.2 Planar surface with local response

In a previous paper, Henkel and co-workers have shown that in the vacuum above a planar dielectric surface at temperature T , described by a local permittivity ε_2 , the spatial coherence function is of the form [5] (see also [18, 19])

$$\mathcal{E}_{ij}(\mathbf{r}_1, \mathbf{r}_2) = \frac{\Theta(\omega, T)}{2\pi\varepsilon_0\omega\tilde{r}^5} \text{Im} \frac{\varepsilon_2 - 1}{\varepsilon_2 + 1} \begin{pmatrix} \tilde{r}^2 - 3\rho^2 & 0 & 3\rho(z_1 + z_2) \\ 0 & \tilde{r}^2 & 0 \\ -3\rho(z_1 + z_2) & 0 & 3(z_1 + z_2)^2 - \tilde{r}^2 \end{pmatrix} \quad (4)$$

where $\Theta(\omega, T) = \hbar\omega/(e^{\hbar\omega/kT} - 1)$. We assume that the field is observed in vacuum (relative permittivity $\varepsilon_1 = 1$). The surface is given by $z = 0$. We have chosen the x -axis such that $\mathbf{r}_1 - \mathbf{r}_2$ lies in the xz -plane and $\rho = x_1 - x_2$. The quantity $\tilde{r}^2 = \rho^2 + (z_1 + z_2)^2$ is the (squared) distance between \mathbf{r}_1 and the image point of \mathbf{r}_2 across the interface.

Eq.(4) applies to leading order when both distances z_1, z_2 are much smaller than the wavelength λ ; for other regimes and higher order corrections, see Ref.[5] and, at $\rho = 0$, Ref.[20]. In the following, we focus on the correlation function at a constant height $z = z_1 = z_2$ and discuss its dependence on the lateral separation ρ ; note that ρ can be positive or negative. The normalized coherence function (4) is qualitatively similar to a Lorentzian: the yy -component, for example, follows a law $\sim [4z^2 + \rho^2]^{-3/2}$. The spatial coherence length is thus equal to z , and decreases without apparent limitation as the surface is approached. The electric energy density derived from (4) diverges like $1/z^3$:

$$u_E(z) = [\Theta(\omega, T)/(8\pi z^3)] \text{Im}[(\varepsilon_2 - 1)/(\varepsilon_2 + 1)]. \quad (5)$$

Both points have been noted by Rytov and co-workers [2], who have also argued that this unphysical result is due to the assumption of a local dielectric response down to the smallest scales. A cutoff would occur naturally in a non-local treatment or taking into account the atomistic structure of the material. This is what we show here in detail, using two different model calculations. Doing this, we also provide a basis for the phenomenological cutoff introduced recently by Kittel and co-workers [13] in the context of heat transfer from a hot, sharp tip into a cold, planar substrate.

2.3 Overview

We will use two models to calculate the coherence function. In both, we focus, as mentioned before, on the fields near a planar surface and compute the field correlations in the vacuum above it, at sub-wavelength distances.

The first model is based on the fluctuation electrodynamics introduced by Ryttov and co-workers [2] where the sources of the field are described by fluctuating polarization currents below the surface. This approach relies on the fluctuation-dissipation theorem that links the spectrum of the polarization current to the dielectric function of the material below the surface. We argue that the currents are spatially correlated on a scale equal to or larger than the material's microscopic lattice constant. We then show that the radiation generated outside the surface shows a minimum coherence length given by this scale; this cuts off the divergences appearing in a local description of the material, as noted in Refs.[2, 13]. This model can be applied to polar ionic crystals in the frequency domain where the dielectric response is dominated by phonon-polariton resonances. It can also cover a non-equilibrium situation where the surface is heated to a different temperature or shows weak temperature gradients [21, 22].

The second model describes the dielectric response of an electron plasma and applies to the plasmon-polariton resonances occurring in metals. We use here directly the fluctuation-dissipation theorem for the electric field [23, 24], restricting ourselves to a field-matter system in “global equilibrium”. The coherence function is determined by reflection coefficients from the surface for which we take the Lindhard form, taking into account the non-local response of the electron plasma. It is shown that the field's coherence length is limited by the Thomas-Fermi screening length, but significant deviations from the local description occur already on the (typically larger) scale of the electron mean free path.

3 Polar crystal

3.1 Current correlations

We assume here that the fluctuating currents that generate the radiation field, are correlated below a certain distance l . Above this distance, the medium response can be considered as local. A lower limit for l is certainly the lattice period a : at scales smaller than a , the concept of a continuous material characterized by a dielectric constant does not make sense any more.

In this situation, the cross correlation spectrum of the fluctuating currents, as given by the fluctuation-dissipation theorem, is no longer delta-correlated in space. We choose here to smoothen the spatial delta function into a gaussian. The fluctuation-dissipation theorem for the currents thus takes the form

$$\langle j_k^*(\mathbf{r}_1, \omega) j_l(\mathbf{r}_2, \omega') \rangle = 2\omega\epsilon_0 \text{Im}[\varepsilon(\bar{\mathbf{r}})] \frac{e^{-(\mathbf{r}_1 - \mathbf{r}_2)^2/l^2}}{\pi^{3/2} l^3} \Theta(\omega, T) \delta_{kl} \delta(\omega - \omega'), \quad (6)$$

where $\bar{\mathbf{r}} = \frac{1}{2}(\mathbf{r}_1 + \mathbf{r}_2)$. The gaussian form for the spatial smoothing is chosen for convenience; another functional dependence, e.g. the model put forward by Kliewer and Fuchs [25], will lead to qualitatively similar results.

3.2 Transmitted field

We then write the cross correlation spectrum for the electric field in terms of Green functions and the currents. We use the convention

$$E_i(\mathbf{r}, \omega) = i\mu_0\omega \int d^3\mathbf{r}' \sum_k G_{ik}(\mathbf{r}, \mathbf{r}'; \omega) j_k(\mathbf{r}', \omega). \quad (7)$$

To proceed further in the calculation, the Green function is written as a Weyl plane wave expansion ([26] and appendix). In the present case, the Green function relates the current on one side of an interface to the electric field on the other side of the interface. It depends on the Fresnel transmission coefficients through this interface.

Using (6) and integrating over the half-space filled with the dielectric, one obtains

$$\begin{aligned} \mathcal{E}_{ij}(\mathbf{r}_1, \mathbf{r}_2) = & 2\mu_0\Theta(\omega, T)\omega \int_0^{2\pi} \frac{d\theta}{2\pi} \int_0^\infty \frac{K \operatorname{Re}(\gamma_2) dK}{2\pi |\gamma_2|^2} \\ & \times e^{-iK\rho \cos \theta} e^{-2\operatorname{Im}(\gamma_1)z} e^{-K^2 l^2/4} e^{-\operatorname{Re}(\gamma_2)^2 l^2/4} g_{ik}^*(\mathbf{K}) g_{jk}(\mathbf{K}) \end{aligned} \quad (8)$$

In the preceding equation, the wavenumber in the medium $i = 1, 2$ is $\mathbf{k}_i = (\mathbf{K}, \gamma_i)$ where $\mathbf{K} = K \cos \theta \mathbf{e}_x + K \sin \theta \mathbf{e}_y$ and $\gamma_i^2 = \epsilon_i(\omega/c)^2 - k^2$. The tensor $g_{ij}(\mathbf{K})$ is related to the Green tensor and defined in the Appendix.

The cross-spectral correlation function depends on four characteristic lengths: the wavelength λ , the distance to the interface z , the locality distance l and the separation ρ between the field points. The latter is the variable considered in our problem. At the wavelengths we work with, we always have $l \ll \lambda$. When z is larger than λ (in the far field), the factor $e^{-2\operatorname{Im}(\gamma_1)z}$ actually limits the integration over K to $0 \leq K \leq \omega/c$, i.e., to propagating waves. The cross-spectral correlation function, in this regime, drops to 0 when ρ exceeds $\lambda/2$, as in the blackbody radiation field. In the intermediate regime $l \ll z \ll \lambda$, the integral is dominated by the range $\omega/c \ll K \ll 1/l$, where the exponentials containing l are close to unity. Hence, the results of Ref.[5] are recovered. Finally, when $z \ll l$, $e^{-2\operatorname{Im}(\gamma_1)z}$ and $e^{-\operatorname{Re}(\gamma_2)^2 l^2/4}$ both approach unity in the relevant range $|\sqrt{\epsilon_2}|\omega/c \ll K < 1/l$. This is the regime we discuss in more detail in the following.

We note in passing that we use our calculation is based on the solution to the transmission problem valid for a local medium. Actually, this solution applies when the wave vector K is smaller than $1/l$ when the medium can be described as homogeneous. But from (8) one sees that whatever the values of z , there is anyway a cut-off in the integration over K at approximately $1/l$. Therefore, one might consider that the local expression of the Fresnel coefficients remains valid. We believe that our model, even if it not rigorously accurate, is useful in view of the insight one gains from the analytic result.

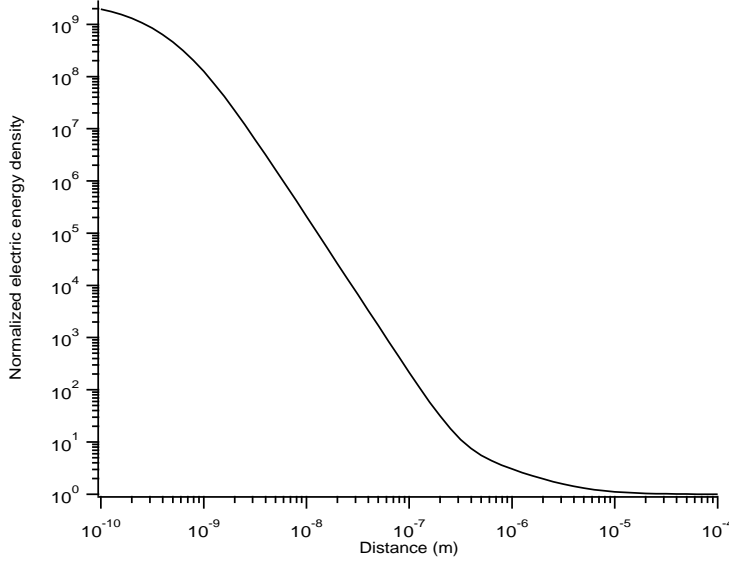


Fig. 1 Normalized electric energy density above a surface of silicon carbide vs. the distance z to the surface. The electric energy density is normalized to the electric energy density in the far field. The locality scale is taken as $l = 1\text{nm}$. The SiC permittivity is described by an oscillator model in the visible-infrared part of the spectrum [28].

3.3 Asymptotics and discussion

Using the limit of $g_{ij}(K)$ for large K , we obtain from (8) the following asymptotic expression for the cross spectral correlation tensor

$$\begin{aligned} \mathcal{E}_{ij}(\mathbf{r}_1, \mathbf{r}_2) &\approx \frac{8\Theta(\omega, T)\text{Im}(\varepsilon_2)}{\varepsilon_0\pi\omega|\varepsilon_2+1|^2l^3} \\ &\times \begin{pmatrix} \frac{\sqrt{\pi}}{2}[M_{3/2} - \frac{3}{4}\frac{\rho^2}{l^2}M_{5/2}] & 0 & -2\frac{\rho}{l}e^{-\rho^2/l^2} \\ 0 & \frac{\sqrt{\pi}}{2}[M_{3/2} + \frac{3}{4}\frac{\rho^2}{l^2}M_{5/2}] & 0 \\ 2\frac{\rho}{l}e^{-\rho^2/l^2} & 0 & \sqrt{\pi}M_{3/2} \end{pmatrix}, \end{aligned} \quad (9)$$

where $M_{3/2} = M(\frac{3}{2}, 1, -\frac{\rho^2}{l^2})$ and $M_{5/2} = M(\frac{5}{2}, 3, -\frac{\rho^2}{l^2})$, and $M(a, b, z)$ is the confluent hypergeometric function [27]. When $\rho \ll l$, $M_{3/2}$ and $M_{5/2}$ both approach unity. Putting $\rho = 0$ in the cross-spectral correlation tensor and taking the trace, we get the electric energy density versus z :

$$z \ll l : \quad u_E(z) = \frac{2\Theta(\omega, T)}{\pi^{1/2}\omega l^3} \text{Im} \frac{\varepsilon_2 - 1}{\varepsilon_2 + 1}. \quad (10)$$

It appears (see Fig.1) that it saturates at short z to a quantity that only depends on l as $1/l^3$: the non-locality scale l thus sets the ultimate length below which the field properties are “frozen” to their value for $z \approx l$.

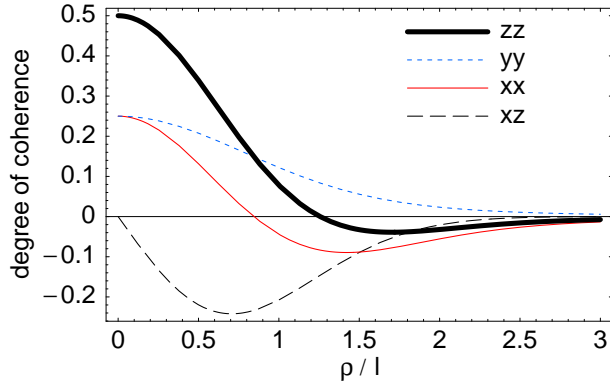


Fig. 2 Normalized spatial coherence function vs. lateral separation ρ in units of the nonlocality scale l . The nonzero components in Eq.(9) are plotted and normalized to the trace of the coherence tensor.

When $\rho \gg l$, all the components of the correlation tensors drop to zero, see Fig.2. This decrease is exponentially fast for the xz and zx components. For the other components, the asymptotic behaviour for large ρ simply scales like $1/\rho^3$ and does not depend on l anymore. This follows from the large argument asymptotics $M_{3/2} \approx \frac{-1}{2\sqrt{\pi}} \frac{l^3}{\rho^3}$ and $M_{5/2} \approx \frac{2}{\sqrt{\pi}} \frac{l^5}{\rho^5}$. Note that in this case, we recover an algebraic decay similar to the local medium case given in Eq.(4).

To summarize this section, we have shown that when we take into account the non-local nature of matter by introducing a locality length l for the sources of the field, the correlation length is about l when the distance to the interface $z < l$. In this regime, the energy density saturates to a value given by the electrostatic energy density expression taken in $z = l$.

4 Nonlocal plasma

We consider in this section another simple situation where the field correlation function can be calculated fairly easily. Restricting ourselves to a field in thermal equilibrium between field and surface, we use directly the fluctuation-dissipation theorem for the field. The relevant information is thus encoded in the electric Green tensor (i.e., the field's response function). The Green tensor contains a part due to the reflection from the surface that is actually dominating in the sub-wavelength distance regime we are interested in. We first review the corresponding reflection coefficients for an electron plasma, taking into account the finite response time of the electrons and their scattering. These two effects make the plasma behave like a nonlocal medium and give rise to the so-called anomalous skin effect. We then discuss the large-wavevector asymptotics of the reflection coefficients and the corresponding limits on the spatial coherence function. It turns out that the scattering mean free path is one key quantity that limits the coherence length at short observation distances.

4.1 Reflection coefficients

We focus here on the electronic contribution to the dielectric function and describe the background ions, interband absorption etc. by a local permittivity ε_b to avoid unnecessary complications. As is well known [29], the dielectric function of a bulk plasma is actually a tensor with two distinct spatial Fourier coefficients, a “longitudinal” $\varepsilon_l(q)$ and a “transverse” $\varepsilon_t(q)$ where q is the modulus of the wavevector. (As before, we suppress the frequency dependence for simplicity.) The fields outside the metal surface are characterized by the reflection coefficients $r_{s,p}(K)$ that depend only on the magnitude $K = |\mathbf{K}|$ of the incident wavevector projected onto the interface. Out of the two polarizations s and p , we need in the following only $r_p(K)$ in the (non-retarded) regime $K \gg \omega/c$. This coefficient is given, e.g., in the review paper by Ford and Weber [30]:

$$r_p(K) = \frac{1/Z_p(K) - 1}{1/Z_p(K) + 1} \quad (11)$$

We use here a dimensionless surface impedance $Z_p(K)$ that reads in the non-retarded limit

$$Z_p(K) = 4K \int_0^\infty \frac{dk_z}{2\pi} \frac{1}{q^2 \varepsilon_l(q)}, \quad q^2 = K^2 + k_z^2, \quad (12)$$

it involves the longitudinal dielectric function only for which we take the Lindhard formula [30, 31]

$$\varepsilon_l(q) = \varepsilon_b + \frac{3\Omega^2}{\omega + i\nu} \frac{u^2 f_l(u)}{\omega + i\nu f_l(u)} \quad (13)$$

$$u = \frac{\omega + i\nu}{qv_F} \equiv \frac{1}{q\ell} \quad (14)$$

$$f_l(u) = 1 - \frac{u}{2} \log \left(\frac{u+1}{u-1} \right). \quad (15)$$

The plasma frequency is given by $\Omega^2 = ne^2/(m\varepsilon_0)$ with $n, -e, m$ the electron density, charge, and mass, respectively.

From the nonlocal permittivity (13–15), two characteristic length scales can be read off: the mean free path $l_{\text{mfp}} = v_F/\nu$ and v_F/ω , the maximum distance over which an electron at the Fermi energy can move ballistically during one period of the applied electric field. In the following, we use the complex length $\ell = v_F/(\omega + i\nu)$ defined in (14) to simplify the notation.

The Lindhard formula, Eqs. (13–15), is based on a semiclassical description of the electron gas (classical particles with Fermi statistics) with a damping rate ν and a velocity v_F at the Fermi energy. This description is valid as long as q is much smaller than the Fermi wave vector $k_F = mv_F/\hbar$. Our model thus applies reasonably well to a “clean metal” where the mean free path is much longer than the Fermi wavelength, and to distances above $1/k_F$ (typically a few Å). Ref.[30] gives a more general dielectric function that covers the regime $q \geq k_F$ as well.

4.2 Coherence function

The fluctuation-dissipation theorem for the electric field, combined with the Green tensor describing the reflection from a planar surface, gives the following integral representation for the field's coherence function:

$$\mathcal{E}_{ij}(\mathbf{r}_1, \mathbf{r}_2) = \mu_0 \omega \Theta(\omega, T) \int_0^\infty \frac{K dK}{2\pi} \sum_{\mu=s,p} \mathcal{C}_{ij}^{(\mu)}(K\rho) \operatorname{Re} \frac{r_\mu(K) e^{2i\gamma_1 z}}{\gamma_1} \quad (16)$$

with $\gamma_1 = (\omega^2/c^2 - K^2)^{1/2}$ ($\operatorname{Im} \gamma_1 \geq 0$). For more details, see for example [32, 33]. We have omitted the free-space part of the Green tensor that gives the same result as for the blackbody field. This part actually becomes negligible compared to the surface part given here if we focus on the sub-wavelength regime, $z_1 = z_2 = z \ll \lambda$: the integration domain $\omega/c \leq K < \infty$ (which is absent in the free-space field) then makes the dominant contribution to the integral.

The tensors $\mathcal{C}_{ij}^{(\mu)}(K\rho)$ in (16) depend on the lateral (signed) distance $\rho = x_1 - x_2$, as introduced after Eq.(4). In p-polarization, it is given by

$$\mathcal{C}^{(p)}(K\rho) = \frac{K^2 c^2}{2\omega^2} \begin{pmatrix} J_0 - J_2 & 0 & 2J_1 \\ 0 & J_0 + J_2 & 0 \\ -2J_1 & 0 & 2J_0 \end{pmatrix}, \quad (17)$$

involving the Bessel functions $J_n = J_n(K\rho)$, $n = 0, 1, 2$. A similar expression applies in s-polarization. We can focus, for short vertical distances, on the range $\omega/c \ll K$, expand the reflection coefficients and find that $|r_s| \ll |r_p|$; hence, the s-polarization is neglected in the following. This also justifies our taking the non-retarded limit of the reflection coefficient (11). To the same accuracy, we approximate $\gamma_1 \approx i|K|$. Finally, the correlation tensor becomes

$$\mathcal{E}_{ij}(\mathbf{r}_1, \mathbf{r}_2) = \mu_0 \omega \Theta(\omega, T) \int_0^\infty \frac{dK}{2\pi} e^{-2Kz} \sum_{\mu=s,p} \mathcal{C}_{ij}^{(\mu)}(K\rho) \operatorname{Im} r_\mu(K). \quad (18)$$

We anticipate from the integral representation (18) that the wave-vector dependence of $\operatorname{Im} r_p(K)$ determines the spatial coherence length: if K_c is the scale on which $\operatorname{Im} r_p(K) \rightarrow 0$, we expect that the divergence of the energy density is smoothed out for $z \ll 1/K_c$ and that the lateral coherence length remains finite: $\ell_{\text{coh}} \sim 1/K_c$ for $z \leq 1/K_c$.

4.3 Local medium

Let us illustrate first how the Lindhard reflection coefficient reduces to its local form (the Fresnel formula). If the q -dependence of $\varepsilon_l(q)$ can be neglected, writing $\varepsilon_l(q) \rightarrow \varepsilon_{\text{loc}}$, the surface impedance (12) integrates to $Z_p \rightarrow 1/\varepsilon_{\text{loc}}$. Eq.(11) then recovers the reflection coefficient for electrostatic images, $r_p \rightarrow (\varepsilon_{\text{loc}} - 1)/(\varepsilon_{\text{loc}} + 1)$ which is the large K limit of the Fresnel formula for transverse magnetic (TM or

p) polarization. The integration of the Bessel functions and exponentials over K in Eq.(18) can be carried out, and we get Eq.(4) with its unphysical $1/z^3$ divergence.

The same divergence would be obtained here from the background permittivity ε_b that we assume local. To focus on the nonlocal contribution from the electron plasma, we consider the regime where ε_b is real so that the leading-order, local contribution analogous to Eq.(4) vanishes.

4.4 Nonlocal reflection coefficient

To get a qualitative insight into the impact of nonlocality, we perform an asymptotic analysis of the dielectric function (13–15):

$$\varepsilon_l(q) \approx \begin{cases} \varepsilon_b - \frac{\Omega^2}{\omega(\omega + i\nu)} \left[1 + (q\ell)^2 \left(\frac{3}{5} + \frac{i\nu}{3\omega} \right) \right], & |q\ell| \ll 1 \\ \varepsilon_b \left(1 + \frac{1}{q^2 \Lambda^2} \right) + \frac{iC}{q^3}, & |q\ell| \gg 1 \end{cases} \quad (19)$$

where

$$\Lambda = \sqrt{\varepsilon_b v_F^2 / (3\Omega^2)} \quad (20)$$

is the Thomas-Fermi length that provides another length scale, and we use the notation $C = 3\pi\omega\Omega^2/v_F^3$. We recall that ℓ is the complex characteristic length defined in (14). Note that for small q , we recover the usual, local Drude expression for an electron plasma

$$\varepsilon_{\text{loc}} = \varepsilon_b - \frac{\Omega^2}{\omega(\omega + i\nu)}. \quad (21)$$

At large q , one gets the dielectric function for Thomas-Fermi screening [29] with a screening length on the order of v_F/Ω plus an imaginary correction.

From the integral (12) for the surface impedance, we find that the typical wavenumber is of the order of $q \geq K$. Hence the two limits quoted above translate into the following asymptotics of the reflection coefficient, after performing the integrations,

$$\text{Im } r_p(K) \approx \begin{cases} \text{Im} \frac{\varepsilon_{\text{loc}} - 1}{\varepsilon_{\text{loc}} + 1}, & |K\ell| \ll 1, \\ \frac{4}{3\varepsilon_b^2} \frac{CK\Lambda^4 g(K\Lambda)}{\left| 1 + K/(\varepsilon_b \sqrt{K^2 + 1/\Lambda^2}) \right|^2}, & |K\ell| \gg 1. \end{cases} \quad (22)$$

The dimensionless function $g(K\Lambda)$ is the integral

$$g(K\Lambda) = \int_0^\infty \frac{dt}{\sqrt{(K\Lambda)^2 + t^2} [(K\Lambda)^2 + 1 + t^2]^2}. \quad (23)$$

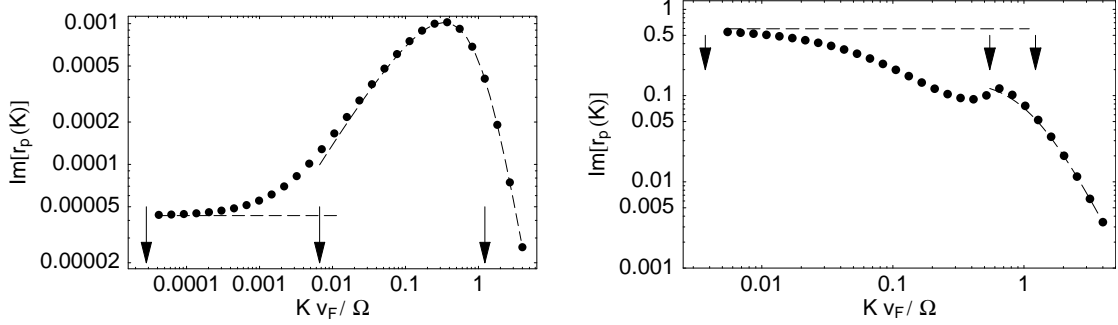


Fig. 3 Reflection coefficient $\text{Im } r_p(K)$ vs. the normalized wave vector Kv_F/Ω . Dashed lines: asymptotical formulas (22). Symbols: numerical calculation. The arrows mark, from left to right, the characteristic scales ω/c , $1/|\ell|$ and $1/\Lambda$. Chosen parameters: $\Omega/\nu = 192$, $c/v_F = 148$, ($v_F/\Omega = 0.84 \text{ \AA}$), taken from the Drude description of aluminium [29]. We take $\varepsilon_b = 2$ to model the contribution of bound electrons. Left panel: $\omega = 0.8 \nu$ or $\lambda = 19 \mu\text{m}$. Right panel: $\omega = 0.55 \Omega$ ($\lambda = 140 \text{ nm}$), near the large- K asymptote of the surface plasmon resonance in the local approximation (given by $\varepsilon_{\text{loc}} + 1 = 0$).

This can be evaluated in closed, but barely instructive form involving a hypergeometric function; its limiting behaviour is

$$\begin{aligned} g(K\Lambda) &\approx \ln(1/K\Lambda) + \ln 2 - \frac{1}{2} \quad \text{for } K\Lambda \ll 1, \\ g(K\Lambda) &= \frac{2}{3}(K\Lambda)^{-4} \quad \text{for } K\Lambda \gg 1. \end{aligned} \quad (24)$$

The first line applies to the intermediate case $1/|\ell| \ll K \ll 1/\Lambda$, the second one to the regime $K \gg 1/\Lambda, 1/|\ell|$. In both cases, Eq.(22) implies that $|\text{Im } r_p(K)| \ll 1$.

The reflection coefficient is plotted in Fig.3 where the asymptotic expressions (22) are represented as dashed lines. We find good agreement outside the crossover range $K|\ell| \sim 1$. In the frequency range of the anomalous skin effect, $\omega \sim \nu$ (left panel, $\lambda = 19 \mu\text{m}$ in the infrared), the nonlocal plasma shows an increased $\text{Im } r_p(K)$, with a cutoff occurring beyond $K_c \sim 1/\Lambda$ [see Eq.(24)]. This effect is well known [30] and is related to the enhanced spontaneous emission rate for a nonlocal metallic surface that was recently pointed out [34]. The reflection loss remains small in absolute numbers because of the large conductivity of the material. The opposite behaviour is found near the (local, non-retarded) surface plasmon resonance (right panel, $\lambda = 140 \text{ nm}$ in the far UV): $\text{Im } r_p(K)$ decreases from its local value, with a weakly resonant feature emerging around $K \sim 1/|\ell|$.

From these plots, we observe that the characteristic wave vector scale K_c strongly depends on the frequency range. An upper limit is set by $1/\Lambda$, involving the Thomas-Fermi screening length, but significant changes already occur on the scale $1/|\ell|$. The characteristic distance below which non-local effects become manifest, is thus given by the largest of $|\ell|$ and Λ . This is typically $|\ell|$, since in order of magnitude, $|\ell|/\Lambda \sim \Omega/|\omega + i\nu|$ which is much larger than unity for good conductors up to the visible domain. At frequencies smaller (larger) than the damping rate ν , the mean free path l_{mfp} (the ‘‘ballistic amplitude’’ v_F/ω): sets the scale for nonlocal effects, respectively.

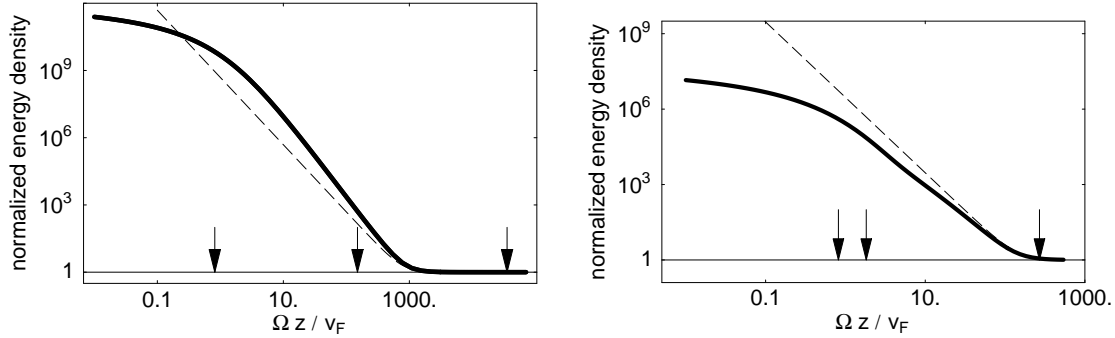


Fig. 4 Electric energy density, normalized to its far-field value, vs. normalized distance $\Omega z / v_F$. Dashed line: local dielectric. Solid line: numerical calculation (left: $\omega = 0.8 \nu$; right: $\omega = 0.55 \Omega$; other parameters as in Fig.3). The arrows mark, from left to right, the characteristic distances Λ , $|\ell|$, and $\lambda = 2\pi c/\omega$.

We note that for typical metals, the Thomas-Fermi scale Λ does not differ much from the Fermi wavelength $1/k_F$. The asymptotics derived above within the semiclassical Lindhard model (13) is therefore only qualitatively valid at short distances (large wavevectors).

4.5 Energy density and lateral coherence

The numerical calculation of the correlation function Eq.(18) can be done efficiently using a numerical interpolation of $\text{Im } r_p(K)$ that we continue for large and small K using the asymptotics derived above.

We plot in Fig.4 the electric energy density as a function of distance, for the same two frequencies as in Fig.3. Deviations from the local approximation (dashed line) occur at distances smaller than $|\ell|$: enhancement at low frequencies ($\omega \sim \nu$, left panel), suppression near the surface plasmon resonance (right panel), which is consistent with the trends seen in Fig.3. A saturation at small distances is also visible, although it occurs for fairly small values of $\Omega z / v_F$ (where the semi-classical Lindhard function is in practice no longer valid). We note also that for $z \geq \lambda$, the plots are only qualitative since the calculation does not take into account retardation.

Finally, we illustrate the finiteness of the coherence length as the distance of observation enters the nonlocal regime. We plot in Fig.5 the zz -component of the normalized coherence tensor (3), as a function of the lateral separation ρ/z . In the local regime, one gets a universal curve independent of the distance (dashed line). This is no longer true near a nonlocal metal: when Thomas-Fermi screening sets in ($z \leq \Lambda$), the coherence function departs from its local limit, its width (the coherence length) becoming much larger than z .

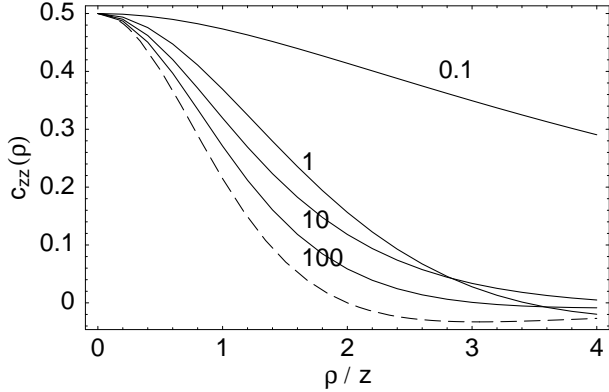


Fig. 5 Normalized degree of spatial coherence for z -polarized fields, probed at a lateral separation ρ . The numbers on the curves (solid lines) give the normalized distance $\Omega z/v_F = 100, 10, 1, 0.1$, with the normalized Thomas-Fermi screening length being $\Omega \Lambda/v_F = (\varepsilon_b/3)^{1/2} \approx 0.8$. Dashed line: result for a local dielectric in the near-field limit $z \ll \lambda$, taken from Eq.(4). The chosen parameters are those of Fig.3, right panel.

5 Concluding remarks

We have discussed in this paper the impact of a nonlocal dielectric response on the spatial coherence of thermal electromagnetic near fields above a planar surface. Using two different models to describe the nonlocal response, we have shown that when the sources of the field have a finite correlation length, this length sets the minimum scale for the coherence length of the field as well. This behaviour is qualitatively similar to what we found previously when investigating the contribution of thermally excited surface plasmons where coherence length and plasmon propagation length coincide [5]. We have thus provided semi-quantitative evidence for the impact of nonlocality that has been conjectured already by Rytov's group [2].

The calculation for an electron plasma model highlights, on the one hand, the crucial role played by Thomas-Fermi screening, that sets the minimum coherence length. On the other hand, significant deviations from the local description already occur at scales below the electron mean free path (Fig.3 and Fig.4), although these are not accompanied by an increase in spatial coherence.

Our calculations can be improved taking into account quantum effects in the Lindhard dielectric function [30], which will lead to quantitative changes at short distance. Indeed, for typical metals, the Thomas-Fermi screening length v_F/Ω and the Fermi wavelength $1/k_F$ are fairly close [29]. A comparison to other models of nonlocal dielectric functions would be interesting as well. On the experimental side, it would be interesting to compare the recent data on heat transfer between a scanning tip and a surface [13] with a microscopic calculation along the lines used here. We also mention that in the context of the Casimir force, nonlocal surface impedances have been studied. The nonlocal correction is particularly relevant at finite temperature and large distances and leads to a behaviour of the Casimir

force that is qualitatively similar, even without absorption, to the local, lossy Drude model, see for example Refs.[35,36]. Finally, it remains to study the impact of another property of real metals, the smooth rather than abrupt transition of the electron density profile at the surface: this can be described by effective surface displacements that depend on both polarization and wave vector, thus adding to the nonlocal effects considered here [37].

We thank Rémi Carminati and Jean-Jacques Greffet for discussion and Illarion Dorofeyev and Francesco Intravaia for helpful comments. C.H. acknowledges support from the European Commission (network FASTNet and projects ACQP and QUELE).

A Appendix

Let us consider the Green tensor relating an electric current in a local medium 2 ($z' < 0$) to the electric field in medium 1 ($z > 0$) that we take as vacuum ($\epsilon_1 = 1$). This tensor can be written as an expansion in plane waves (Weyl expansion)

$$G_{ij}(\mathbf{r}, \mathbf{r}') = \frac{i}{2} \int \frac{d^2 \mathbf{K}}{(2\pi)^2 \gamma_2} g_{ij}(\mathbf{K}) e^{i[k_x(x-x') + k_y(y-y')]} e^{i\gamma_1 z} e^{-i\gamma_2 z'}, \quad (25)$$

where $\mathbf{K} = (k_x, k_y)$ is the wave vector component parallel to the interface. The γ_i are the z -components of the wave vector: $\gamma_i^2 = \epsilon_i(\omega/c)^2 - K^2$. In the notation of Ref.[5],

$$g_{ij}(\mathbf{K}) = \sum_{\mu=s,p} e_{\mu,i}^{(t)} e_{\mu,j}^{(2)} t_{\mu}^{21} \quad (26)$$

The polarization vectors for the s and p polarization are

$$\mathbf{e}_s^{(t)} = \mathbf{e}_s^{(2)} = \hat{\mathbf{K}} \times \hat{\mathbf{e}}_z \quad (27)$$

$$\mathbf{e}_p^{(t)} = \frac{K \hat{\mathbf{z}} - \gamma \hat{\mathbf{K}}}{\omega/c} \quad (28)$$

$$\mathbf{e}_p^{(2)} = \frac{K \hat{\mathbf{z}} - \gamma_2 \hat{\mathbf{K}}}{\sqrt{\epsilon_2} \omega/c} \quad (29)$$

where $\hat{\mathbf{K}}$ is the unit vector parallel to \mathbf{K} . The t_{μ}^{21} are the Fresnel transmission coefficients between media 2 and 1:

$$t_s^{21} = \frac{2\gamma_2}{\gamma_1 + \gamma_2}, \quad t_p^{21} = \frac{2\gamma_2 \sqrt{\epsilon_2}}{\epsilon_2 \gamma_1 + \gamma_2}. \quad (30)$$

References

1. M. Planck: Verh. Dt. phys. Ges. (Berlin) **2**, 237 (1900)
2. S. M. Rytov, Y. A. Kravtsov, V. I. Tatarskii: *Elements of Random Fields*, Vol. 3 of *Principles of Statistical Radiophysics*. Berlin: Springer 1989
3. F. Gori, D. Ambrosini, V. Bagini: Opt. Commun. **107**, 331 (1994)
4. R. Carminati, J.-J. Greffet: Phys. Rev. Lett. **82**, 1660 (1999)

5. C. Henkel, K. Joulain, R. Carminati, J.-J. Greffet: Opt. Commun. **186**, 57 (2000)
6. O. D. Stefano, S. Savasta, R. Girlanda: Phys. Rev. A **60**, 1614 (1999)
7. R. R. Chance, A. Prock, R. Silbey: in *Advances in Chemical Physics XXXVII*, edited by I. Prigogine, S. A. Rice. New York: Wiley & Sons 1978, pp. 1–65
8. R. C. Dunn: Chem. Rev. **99**, 2891 (1999)
9. F. Chen, U. Mohideen, G. L. Klimchitskaya, V. M. Mostepanenko: Phys. Rev. Lett. **88**, 101801 (2002)
10. J.-B. Xu, K. Lauger, R. Moller, K. Dransfeld, I. H. Wilson: J. Appl. Phys. **76**, 7209 (1994)
11. J. B. Pendry: J. Phys. Cond. Matt. **11**, 6621 (1999)
12. J.-P. Mulet, K. Joulain, R. Carminati, J.-J. Greffet: Appl. Phys. Lett. **78**, 2931 (2001)
13. A. Kittel, W. Müller-Hirsch, J. Parisi, S.-A. Biehs, D. Reddig, M. Holthaus: Phys. Rev. Lett. **95**, 224301 (2005)
14. L. Mandel, E. Wolf: *Optical coherence and quantum optics*. Cambridge: Cambridge University Press 1995
15. K. Joulain, R. Carminati, J.-P. Mulet, J.-J. Greffet: Phys. Rev. B **68**, 245405 (2003)
16. T. Setälä, M. Kaivola, A. T. Friberg: Phys. Rev. Lett. **88**, 123902 (2002)
17. J. Ellis, A. Dogariu, S. Ponomarenko, E. Wolf: Opt. Lett. **29**, 1536 (2004)
18. C. Girard, C. Joachim, S. Gauthier: Rep. Prog. Phys. **63**, 893 (2000)
19. C. Henkel: *Coherence theory of atomic de Broglie waves and electromagnetic near fields*. Potsdam: Universitätsverlag 2004, online at <http://opus.kobv.de/ubp/volltexte/2005/135/>
20. S. Scheel, L. Knöll, D.-G. Welsch: acta phys. slov. **49**, 585 (1999) [quant-ph/9905007].
21. D. Polder, M. V. Hove: Phys. Rev. B **4**, 3303 (1971)
22. C. H. Henry, R. F. Kazaninov: Rev. Mod. Phys. **68**, 801 (1996)
23. H. B. Callen, T. A. Welton: Phys. Rev. **83**, 34 (1951)
24. W. Eckhardt: Opt. Commun. **41**, 305 (1982)
25. K. L. Kliewer, R. Fuchs: Adv. Chem. Phys. **27**, 355 (1974)
26. J. M. Wylie, J. E. Sipe: Phys. Rev. A **30**, 1185 (1984)
27. *Handbook of Mathematical Functions*, ninth ed., edited by M. Abramowitz, I. A. Stegun. New York: Dover Publications, Inc. 1972
28. *Handbook of optical constants of solids*, edited by E. Palik. San Diego: Academic 1985
29. N. W. Ashcroft, N. D. Mermin: *Solid State Physics*. Philadelphia: Saunders 1976
30. G. W. Ford, W. H. Weber: Phys. Rep. **113**, 195 (1984)
31. K. L. Kliewer, R. Fuchs: Phys. Rev. **172**, 607 (1968)
32. G. S. Agarwal: Phys. Rev. A **11**, 230 (1975)
33. I. Dorofeyev, H. Fuchs, J. Jersch: Phys. Rev. E **65**, 026610 (2002)
34. I. A. Larkin, M. I. Stockman, M. Achermann, V. I. Klimov: Phys. Rev. B **69**, 121403(R) (2004)
35. V. B. Svetovoy, R. Esquivel: Phys. Rev. E **72**, 036113 (2005)
36. B. E. Sernelius: Phys. Rev. B **71**, 235114 (2005)
37. P. J. Feibelman: Progr. Surf. Sci. **12**, 287 (1982)